

Top quark pair production via polarized and unpolarized photons in Supersymmetric QCD

Han Liang^{b,*}, Ma Wen-Gan^{a,b}, Yu Zeng-hui^b

^aCCAST (World Laboratory), P.O.Box 8730, Beijing 100080, P.R.China

^bDepartment of Modern Physics, University of Science and Technology of China (USTC), Hefei, Anhui 230027, P.R.China, [†]

ABSTRACT

QCD corrections to top quark pair production via fusion of both polarized and unpolarized photons are calculated in Supersymmetric Model. The corrections are found to be sizable. The dependence of the corrections on the masses of the supersymmetric particles is also investigated. Furthermore, we studied CP asymmetry effects arising from the complex couplings in the MSSM. The CP violating parameter can reach 10^{-2} for favorable parameter values.

PACS number(s): 13.65.+i, 13.88.+e, 14.65.-q, 14.80.Dq, 14.80.Gt

*email:rdhan@hpe25.nic.ustc.edu.cn

[†]Mailing address

I. Introduction

Direct evidence for the top quark was recently presented by the CDF (Collider Detector at Fermilab) Collaboration [1]. This is considered to be a remarkable success for the Standard Model (SM), since the value of the top mass determined by them, $174 \pm 10_{-12}^{+13} \text{ GeV}$, coincides with the indirect determination from the available precise data of electroweak experiments. Due to the determination of the top quark mass, it is certain that a number of new and interesting issues in top quark pair production and decay will arise. At the Next Linear Collider (NLC), operating in photon-photon collision mode at a design energy of $500 \sim 2000 \text{ GeV}$ with a luminosity of the order $10^{33} \text{ cm}^{-2} \text{ s}^{-1}$ [2], a large number of heavy quark pairs and other new particles can be produced with an agreeable production rate [3]. Those events would be much cleaner than those produced at pp and $p\bar{p}$ colliders. It has been also found that the $t\bar{t}$ production rate in $\gamma\gamma$ collisions from laser back-scattering is much larger than that from the direct $e^+e^- \rightarrow t\bar{t}$ production both with and without considering the threshold QCD effect, for $m_t \sim 100 - 200 \text{ GeV}$ at center-of-mass energies of the electron-positron system around 1 TeV.[4]. Thus the process $\gamma\gamma \rightarrow t\bar{t}$ has a large potential for producing and studying heavy quarks directly. The next-to-leading order QCD corrections in the SM for this process both for polarized and unpolarized particle collisions have been discussed in detail in Ref.[5]. There it was shown that these QCD corrections are significant, about 10%. However, the process also seems to be sensitive in searching for virtual effects from new particles, which

would imply physics beyond the Standard Model. Among various models which introduce new physics, the Minimal Supersymmetric Standard Model (MSSM)[6] is the most attractive one at present, since it is the simplest case of Supersymmetric Models (SUSY). Therefore it is important to study the physical effects induced by the virtual supersymmetric particles for top quark pair production via photon fusion. If we assume that one of the stop quarks are much lighter than the other supersymmetric quarks due to strong mixing, the process $\gamma\gamma \rightarrow t\bar{t}$ would be a very interesting reaction for testing supersymmetric theory in that the corrections due to virtual \tilde{t} would provide evidence for the existence of the quark scalar partners. Recently H. Wang et al. have calculated the Supersymmetric QCD corrections for this process via unpolarized photon collisions in some cases in Ref.[7].

With the advent of new collider techniques, back-scattered laser photons can be linearly polarized with high luminosity and rather high efficiency [8]. These techniques will undoubtedly be used to improve our knowledge of the top quark parameters, particularly when one combines the data from top pair production via photon-photon fusion with other data from e^+e^- and pp collisions. In addition to that general advantage, the process of top quark pair produced by polarized photon collisions may provide us with a better understanding of CP-violation phenomena [9]. Since the mixing of top quarks with other generations is very small, CP-violation in this process is negligibly small within the Kobayashi-Maskawa framework of the Standard Model. However, in the MSSM, even without generation mixing, there

are more possibilities to introduce complex couplings than in the SM. Here in this paper, we limit ourselves only to the combination of the CP-violating phases $\phi_{\tilde{t}}$ and $\phi_{\tilde{g}}$, which emerge in the stop quark mixing matrix and in the Majorana mass term of the gluino [10]. These non-zero complex phases, which occur in the Lagrangian, cannot be rotated away by a suitable redefinition of the fields. They will lead to CP violation within a single generation. Therefore, the observation of CP-violation in the process of top quark pair production via polarized $\gamma\gamma$ fusion may help to promote our understanding of the features of the combination of CP-violating phases $\phi_{\tilde{t}}$ and $\phi_{\tilde{g}}$.

The paper is organized as follows: in Sec. II, the renormalization of the top quark self-energy in the frame of the MSSM is described, and the explicit analytical forms of the Lorentz invariant matrix elements including the next-to-leading order of supersymmetric QCD corrections are presented. In Sec. III, the numerical results and discussions are depicted. Finally, the conclusions are given. In the appendix, the form factors used for the cross section calculations are listed.

II. Calculations

In this work, we denote the reaction discussed as

$$\gamma(p_3, \lambda_1)\gamma(p_4, \lambda_2) \longrightarrow t(p_2)\bar{t}(p_1) \quad (2.1)$$

where $\lambda_{1,2} = \pm 1$, p_2 and p_1 represent the momenta of the outgoing top quark

and its anti-particle, p_3 and p_4 are for the momenta of the two incoming photons with helicities λ_1 and λ_2 respectively.

The Feynman diagrams for the process $\gamma\gamma \rightarrow t\bar{t}$ are shown in Fig.1, and the relevant Feynman rules can be found in [6]. In the calculation dimensional regularization and the on-mass-shell (OMS) renormalization scheme[11] are adopted to eliminate all the ultraviolet divergences. The interaction Lagrangian for gluino-stop-top coupling including the CP-violating phases is given by

$$\begin{aligned} L_{\tilde{g}t\bar{t}} &= -\sqrt{2}g_s T^a \bar{t} [(\cos\theta_{\tilde{t}} \tilde{t}_1 + \sin\theta_{\tilde{t}} \tilde{t}_2) e^{-i\phi} P_R \\ &\quad + (\sin\theta_{\tilde{t}} \tilde{t}_1 - \cos\theta_{\tilde{t}} \tilde{t}_2) e^{i\phi} P_L] \tilde{g}_a + h.c. \\ &= -\sqrt{2}g_s T^a \bar{t} [(A_R \tilde{t}_1 + B_R \tilde{t}_2) P_R + (A_L \tilde{t}_1 - B_L \tilde{t}_2) P_L] \tilde{g}_a + h.c. \end{aligned} \quad (2.2)$$

where g_s is the strong coupling constant, T^a are $SU(3)_C$ generators and $P_{R,L} = \frac{1}{2}(1 \pm \gamma_5)$. $\theta_{\tilde{t}}$ is the stop mixing angle which transforms the stop mass eigenstates \tilde{t}_n ($n=1,2$) to the weak eigenstates \tilde{t}_L and \tilde{t}_R . $\phi = \phi_{\tilde{t}} - \phi_{\tilde{g}}$ is the combination of the two phase angles. In the Equation (2.2) we denote

$$\begin{aligned} A_R &= \cos\theta_{\tilde{t}} e^{-i\phi}, & A_L &= \sin\theta_{\tilde{t}} e^{i\phi}, \\ B_R &= \sin\theta_{\tilde{t}} e^{-i\phi}, & B_L &= \cos\theta_{\tilde{t}} e^{i\phi} \end{aligned} \quad (2.3)$$

With the introduction of the CP-violating phase ϕ in the MSSM, the renormalized one-particle irreducible two-point function for top quarks containing the contributions from SUSY QCD should be written as [12]

$$\hat{\Gamma}(p) = i(\not{p} - m_t) + i \left[\not{p} P_L \hat{\Sigma}^L(p^2) + \not{p} P_R \hat{\Sigma}^R(p^2) + P_L \hat{\Sigma}^S(p^2) + P_R \hat{\Sigma}^S \dagger(p^2) \right]. \quad (2.4)$$

It should be mentioned here that in the above equation the upper conjugation symbol \dagger acts only on the CP-violating phase ϕ . The corresponding unrenormalized top quark self energies read

$$\Sigma^L(p^2) = -\frac{C_F}{8\pi^2}g_s^2 \left(A_R B_L B_1[p^2, m_{\tilde{g}}, m_{\tilde{t}_1}] + A_L B_R B_1[p^2, m_{\tilde{g}}, m_{\tilde{t}_2}] \right), \quad (2.5)$$

$$\Sigma^R(p^2) = -\frac{C_F}{8\pi^2}g_s^2 \left(A_L B_R B_1[p^2, m_{\tilde{g}}, m_{\tilde{t}_1}] + A_R B_L B_1[p^2, m_{\tilde{g}}, m_{\tilde{t}_2}] \right), \quad (2.6)$$

$$\Sigma^S(p^2) = \frac{C_F}{8\pi^2}g_s^2 m_{\tilde{g}} A_L B_L \left(B_0[p^2, m_{\tilde{g}}, m_{\tilde{t}_1}] - B_0[p^2, m_{\tilde{g}}, m_{\tilde{t}_2}] \right), \quad (2.7)$$

$$\Sigma^{S\dagger}(p^2) = \frac{C_F}{8\pi^2}g_s^2 m_{\tilde{g}} A_R B_R \left(B_0[p^2, m_{\tilde{g}}, m_{\tilde{t}_1}] - B_0[p^2, m_{\tilde{g}}, m_{\tilde{t}_2}] \right). \quad (2.8)$$

m_t and $m_{\tilde{t}_n}$ ($n = 1, 2$) involved above are the masses of the top quark and stop mass eigenstates. In the SU(3) group, $C_F = (N_c^2 - 1)/(2N_c)$. Imposing the on-shell renormalization conditions given in Ref.[11], one can obtain equations for the renormalized self-energy functions:

$$m_t \tilde{R}e \hat{\Sigma}^L(m_t^2) + \tilde{R}e \hat{\Sigma}^{S\dagger}(m_t^2) = 0$$

$$m_t \tilde{R}e \hat{\Sigma}^R(m_t^2) + \tilde{R}e \hat{\Sigma}^S(m_t^2) = 0$$

$$m_t \tilde{R}e \hat{\Sigma}^L(m_t^2) + \tilde{R}e \hat{\Sigma}^S(m_t^2) = 0$$

$$\begin{aligned}
& m_t \tilde{R}e \hat{\Sigma}^R(m_t^2) + \tilde{R}e \hat{\Sigma}^{S \dagger}(m_t^2) = 0 \\
& \tilde{R}e \hat{\Sigma}^L(m_t^2) + \tilde{R}e \hat{\Sigma}^R(m_t^2) + 2m_t \frac{\partial}{\partial p^2} \tilde{R}e(m_t \hat{\Sigma}^L(p^2) + m_t \hat{\Sigma}^R(p^2) + \hat{\Sigma}^S(p^2) + \hat{\Sigma}^{S \dagger}(p^2)) \Big|_{p^2=m_t^2} = 0
\end{aligned} \tag{2.9}$$

where $\tilde{R}e$ only takes the real part of the loop integral functions appearing in the self energies. The relevant self-energy and vertex counterterms are

$$\begin{aligned}
i\delta\Sigma &= i[C_L \not{p} P_L + C_R \not{p} P_R - C_S^- P_L - C_S^+ P_R], \\
i\delta\Lambda^\mu &= -ieQ_t \gamma^\mu [C^- P_L + C^+ P_R].
\end{aligned} \tag{2.10}$$

where Q_t is the charge of the top quark and

$$\begin{aligned}
C_L &= C^- = \frac{1}{2}(\delta Z^L + \delta Z^{L\dagger}), \\
C_R &= C^+ = \frac{1}{2}(\delta Z^R + \delta Z^{R\dagger}), \\
C_S^- &= \frac{m_t}{2}(\delta Z^L + \delta Z^{R\dagger}) + \delta m, \\
C_S^+ &= \frac{m_t}{2}(\delta Z^R + \delta Z^{L\dagger}) + \delta m.
\end{aligned} \tag{2.11}$$

We choose the field renormalization constant δZ^R to be real. Using Eq. (2.9)-(2.11), we obtain the renormalization constants as

$$\delta m = \frac{1}{2} \left(m_t \tilde{R}e \Sigma^L(m_t^2) + m_t \tilde{R}e \Sigma^R(m_t^2) + \tilde{R}e \Sigma^S(m_t^2) + \tilde{R}e \Sigma^{S \dagger}(m_t^2) \right), \tag{2.12}$$

$$\begin{aligned}
\delta Z^L &= -\Sigma^L(m_t^2) - \frac{1}{m_t} \left[\tilde{R}e \Sigma^{S \dagger}(m_t^2) - \tilde{R}e \Sigma^S(m_t^2) \right] \\
&\quad - m_t \frac{\partial}{\partial p^2} \left[m_t \tilde{R}e \Sigma^L(p^2) + m_t \tilde{R}e \Sigma^R(p^2) + \tilde{R}e \Sigma^S(p^2) + \tilde{R}e \Sigma^{S \dagger}(p^2) \right] \Big|_{p^2=m_t^2},
\end{aligned} \tag{2.13}$$

$$\delta Z^R = -\Sigma^R(m_t^2) - m_t \frac{\partial}{\partial p^2} \left[m_t \tilde{R}e \Sigma^L(p^2) + m_t \tilde{R}e \Sigma^R(p^2) + \tilde{R}e \Sigma^S(p^2) + \tilde{R}e \Sigma^{S \dagger}(p^2) \right] \Big|_{p^2=m_t^2}, \tag{2.14}$$

Including all next-to-leading order supersymmetric QCD corrections, the renormalized amplitude for $t\bar{t}$ pair production in $\gamma\gamma$ collisions is shown as

$$\begin{aligned}
M_{ren}(\lambda_2, \lambda_1) &= M_0(\lambda_2, \lambda_1) + \delta M^{1-loop}(\lambda_2, \lambda_1) \\
&= M_0(\lambda_2, \lambda_1) + \delta M^{self}(\lambda_2, \lambda_1) + \delta M^{vertex}(\lambda_2, \lambda_1) + \\
&\quad \delta M^{box}(\lambda_2, \lambda_1) + \delta M^{tr}(\lambda_2, \lambda_1)
\end{aligned} \tag{2.15}$$

where M_0 is the amplitude at the tree level, δM^{self} , δM^{vertex} , δM^{box} and δM^{tr} represent the renormalized amplitudes with the next-to-leading order supersymmetric QCD corrections arising from the self-energy, vertex, box and triangle diagrams, respectively. Their explicit forms are given by

$$\begin{aligned}
M_0(\lambda_2, \lambda_1) = & - i \frac{e^2 Q_t^2}{\hat{t} - m_t^2} \epsilon_\mu(p_4, \lambda_2) \epsilon_\nu(p_3, \lambda_1) \bar{u}(p_2) \gamma^\mu (\not{p}_2 - \not{p}_4 + m_t) \gamma^\nu v(p_1) \\
& + (p_3 \leftrightarrow p_4, \mu \leftrightarrow \nu, \hat{t} \rightarrow \hat{u})
\end{aligned} \tag{2.16}$$

$$\begin{aligned}
\delta M^s(\lambda_2, \lambda_1) = & i \frac{e^2 Q_t^2}{(\hat{t} - m_t^2)^2} \epsilon_\mu(p_4, \lambda_2) \epsilon_\nu(p_3, \lambda_1) \sum_{N=L,R} \bar{u}_N(p_2) \\
& (f_{1,N}^{s(\hat{t})} \gamma^\mu \gamma^\nu + f_{2,N}^{s(\hat{t})} p_2^\mu \gamma^\nu + f_{3,N}^{s(\hat{t})} \not{p}_4 \gamma^\mu \gamma^\nu) v(p_1) \\
& + (p_3 \leftrightarrow p_4, \mu \leftrightarrow \nu, \hat{t} \rightarrow \hat{u})
\end{aligned} \tag{2.17}$$

$$\begin{aligned}
\delta M^v(\lambda_2, \lambda_1) = & -i \frac{e^2 Q_t^2}{\hat{t} - m_t^2} \epsilon_\mu(p_4, \lambda_2) \epsilon_\nu(p_3, \lambda_1) \sum_{N=L,R} \bar{u}_N(p_2) \\
& (f_{1,N}^{v(\hat{t})} \gamma^\mu \gamma^\nu + f_{2,N}^{v(\hat{t})} p_1^\nu \gamma^\mu + f_{3,N}^{v(\hat{t})} p_2^\mu \gamma^\nu \\
& + f_{4,N}^{v(\hat{t})} p_1^\nu p_2^\mu + f_{5,N}^{v(\hat{t})} \not{p}_4 \gamma^\mu \gamma^\nu + f_{6,N}^{v(\hat{t})} \not{p}_4 p_1^\nu \gamma^\mu + f_{7,N}^{v(\hat{t})} \not{p}_4 p_2^\mu \gamma^\nu) v(p_1) \\
& + (p_3 \leftrightarrow p_4, \mu \leftrightarrow \nu, \hat{t} \rightarrow \hat{u})
\end{aligned} \tag{2.18}$$

$$\delta M^b(\lambda_2, \lambda_1) = i \frac{2e^2 Q_t^2 g_s^2}{\pi^2} \epsilon_\mu(p_4, \lambda_1) \epsilon_\nu(p_3, \lambda_2) \sum_{N=L,R} \bar{u}_N(p_2)$$

$$\begin{aligned}
& \left[f_{1,N}^{b(\hat{t})} \gamma^\mu \gamma^\nu + f_{2,N}^{b(\hat{t})} \gamma^\nu \gamma^\mu + f_{3,N}^{b(\hat{t})} p_1^\nu \gamma^\mu + f_{4,N}^{b(\hat{t})} p_1^\mu \gamma^\nu \right. \\
& + f_{5,N}^{b(\hat{t})} p_2^\nu \gamma^\mu + f_{6,N}^{b(\hat{t})} p_2^\mu \gamma^\nu + f_{7,N}^{b(\hat{t})} p_1^\mu p_1^\nu + f_{8,N}^{b(\hat{t})} p_1^\mu p_2^\nu + f_{9,N}^{b(\hat{t})} p_2^\mu p_1^\nu \\
& + f_{10,N}^{b(\hat{t})} p_2^\mu p_2^\nu + f_{11,N}^{b(\hat{t})} \not{p}_4 \gamma^\mu \gamma^\nu + f_{12,N}^{b(\hat{t})} \not{p}_4 \gamma^\nu \gamma^\mu + f_{13,N}^{b(\hat{t})} \not{p}_4 p_1^\mu p_1^\nu \\
& \left. + f_{14,N}^{b(\hat{t})} \not{p}_4 p_1^\mu p_2^\nu + f_{15,N}^{b(\hat{t})} \not{p}_4 p_2^\mu p_1^\nu + f_{16,N}^{b(\hat{t})} \not{p}_4 p_2^\mu p_2^\nu \right] v(p_1) \\
& + (p_3 \leftrightarrow p_4, \mu \leftrightarrow \nu, \hat{t} \rightarrow \hat{u})
\end{aligned} \tag{2.19}$$

$$\delta M^{tr}(\lambda_2, \lambda_1) = -i \frac{e^2 Q_t^2 g_s^2}{\pi^2} g^{\mu\nu} \epsilon_\mu(p_4, \lambda_2) \epsilon_\nu(p_3, \lambda_1) \sum_{N=L,R} f_N^{tr} \bar{u}_N(p_2) v(p_1) \tag{2.20}$$

Here $\hat{t} = (p_4 - p_2)^2$, $\hat{u} = (p_1 - p_4)^2$. The explicit form factors $f_{i,N}^{s(\hat{t})}$, $f_{i,N}^{v(\hat{t})}$, $f_{i,N}^{b(\hat{t})}$, f_N^{tr} are presented in the appendix. The analytical deduction for the renormalized amplitudes in Eq.(2.15) clearly states the complete cancellation of ultraviolet divergences, which is required to ensure the correctness of our calculation.

The cross section of the process for the polarized photons is given by

$$\hat{\sigma}^{\lambda_2, \lambda_1}(\hat{s}) = \frac{N_c}{16\pi \hat{s}(\hat{s} - 4m_t^2)} \int_{\hat{t}^-}^{\hat{t}^+} d\hat{t} \sum_{spins} |M_{ren}^{\lambda_2 \lambda_1}(\hat{s}, \hat{t})|^2, \tag{2.21}$$

where N_c is the number of colors, $\hat{t}^\pm = (m_t^2 - \frac{1}{2}\hat{s}) \pm \frac{1}{2}\hat{s}\beta_t$, $\beta_t = \sqrt{1 - 4m_t^2/\hat{s}}$.

Note that the summing over the spins is performed only over the final quark pair:

$$\sum_{spins} |M_{ren}^{\lambda_2, \lambda_1}(\hat{s}, \hat{t})|^2 = \sum_{spins} |M_0^{\lambda_2, \lambda_1}|^2 + 2Re \left(\sum_{spins} M_0^{\lambda_2 \lambda_1 \dagger} \cdot \delta M_{1-loop}^{\lambda_2, \lambda_1} \right). \tag{2.22}$$

For polarized massless vector particles we have

$$\epsilon_{\lambda_2}^\mu(k) \epsilon_{\lambda_1}^{\nu*}(k) = \frac{\delta_{\lambda_2, \lambda_1}}{2} (-g^{\mu\nu} + \frac{p^\mu k^\nu + p^\nu k^\mu}{(p \cdot k)} + i\lambda_2 \epsilon^{\sigma\mu\rho\nu} \frac{k_\sigma p_\rho}{(p \cdot k)}) \tag{2.23}$$

where \mathbf{p} is an arbitrary light-like Lorentz vector.

The cross section with unpolarized photons is

$$\sigma = \frac{1}{4} \sum_{\lambda_1, \lambda_2 = -1}^{+1} \sigma(\lambda_1, \lambda_2). \quad (2.24)$$

III. Numerical results and discussion.

In the numerical evaluation, we take the top quark mass to be $m_t = 175 \text{ GeV}$, $\alpha = 1/137.036$ and use the two-loop running coupling constant α_s . For the MSSM parameters, we assume that the supersymmetric weak eigenstate partners \tilde{t}_L and \tilde{t}_R mix equivalently, namely the mixing angle $\theta_{\tilde{t}} = 45^\circ$. For the other two independent parameters in stop quark mass matrix, we use the masses of the stop mass eigenstates, and assume $m_{\tilde{t}_1} \leq m_{\tilde{t}_2}$. Current experiments [13] constrain the light stop mass eigenstate to be heavier than 50 GeV. To describe CP violation in $t\bar{t}$ production in polarized $\gamma\gamma$ fusion, a CP-violating parameter ξ_{CP} is defined as below:

$$\xi_{CP} = \frac{\sigma(++) - \sigma(--)}{\sigma(++) + \sigma(--)} \quad (3.1)$$

We set the CP-violating phase to be $\phi = 45^\circ$ when evaluating the cross section in the case of non-zero phase angle, so that the CP-violating effect can be maximized.

In Fig.2(a)(b) the corrections for the cross sections $\sigma(\pm\pm)$ and $\sigma(\pm\mp)$ for different initial photon linear polarizations are plotted as functions of the c.m. energy $\sqrt{\hat{s}}$, assuming the following mass values for supersymmetric particles involved:

$$m_{\tilde{g}} = 100 \text{ GeV}, \quad m_{\tilde{t}_1} = 100 \text{ GeV}, \quad m_{\tilde{t}_2} = 450 \text{ GeV} \quad (3.2)$$

Unlike the corrections from the SM [5], all the contributions of the MSSM are negative in all the polarization cases. The relative correction δ , defined as $(\hat{\sigma} - \hat{\sigma}_0)/\hat{\sigma}_0$, is generally in the order of 10^{-2} which is less than that of the Standard Model QCD corrections [5]. But it can also reach about 10% in some points. Fig.2(a) and Fig.2(b) show that the corrections will be suppressed in the case of introducing a non-zero CP-violating phase angle for both of the polarized photon fusion modes under the conditions of Eq.(3.2). The dependence of the CP-violation parameter ξ_{CP} on $\sqrt{\hat{s}}$ is given in Fig.2(c). It shows that in the c.m. energy range around the $t\bar{t}$ threshold, CP is strongly violated, where ξ_{CP} can be above 2.6%. The curve drops sharply with increasing $\sqrt{\hat{s}}$. From the definition of the CP-violating parameter ξ_{CP} given in Eq.(3.1), one can understand that the feature of the curve in Fig.2(c) is simply the result from Fig.2(a,b).

Since the present experimental results can not exclude the existence of very light gluinos and there has been renewed interest in this case recently, we also calculate the relative corrections to the cross sections with a very light gluino mass, as functions of $\sqrt{\hat{s}}$ when

$$m_{\tilde{g}} = 5 \text{ GeV}, \quad m_{\tilde{t}_1} = 50 \text{ GeV}, \quad m_{\tilde{t}_2} = 250 \text{ GeV} \quad (3.3)$$

The relative corrections $\delta(\pm, \pm)$ and $\delta(\pm, \mp)$ for different photon linear polarizations are plotted in Fig.3(a) and Fig.3(b) respectively. The curves go from positive

to negative values as $\sqrt{\hat{s}}$ increases. The relative corrections are positive around $t\bar{t}$ threshold, whereas they are always negative with the conditions Eq.(3.2) where the gluino mass is much heavier. Although in most energy regions the absolute corrections are small compared with the results given in Fig.2(a,b), the maximal value of relative correction is still about 3.5% around $\sqrt{\hat{s}} = 500 \text{ GeV}$ which can be seen in Fig.3(a). The high peaks shown in Fig.3(a) are the results from resonance effect when $\sqrt{\hat{s}} \sim 2m_{\tilde{t}_2} = 500 \text{ GeV}$, which comes from the contributions of the triangle diagrams in Fig.1(i). The CP violation quantities in this case are plotted in Fig.3(c). All the values of ξ_{CP} have negative signs, and are about an order of magnitude lower than the values in Fig.2(c), varying from -0.184% to -0.296% .

As a check, we also calculate the corrections with extending c.m. energy $\sqrt{\hat{s}}$ up to the region between $2 \sim 5 \text{ TeV}$ and taking the same parameters of Eq.(3.2) and Eq.(3.3) respectively. The absolute corrections get smaller with increasing $\sqrt{\hat{s}}$. Noteworthy the convergency of the correction with heavy gluino and squarks is much faster than that with light gluino and squarks. It proves that the decoupling really takes place at high energies, and the results of our cross section spectra at one-loop level satisfy the unitarity which is expected on theoretical grounds.

According to Eq.(2.24), we can get the relationship between the unpolarized cross section and the gluino mass, which is shown in Fig.4(a) with

$$m_{\tilde{t}_1} = 100 \text{ GeV}, \quad m_{\tilde{t}_2} = 450 \text{ GeV} \quad \text{and} \quad \sqrt{\hat{s}} = 500 \text{ GeV} \quad (3.4)$$

From the figure, we can see that the corrections jump abruptly at the point $m_{\tilde{g}} = 75 \text{ GeV}$. This sudden change is due to the influence of a singularity in top quark wave function renormalization at the point $m_t = m_{\tilde{g}} + m_{\tilde{t}_1}$. This singularity originates from the renormalization constants δZ^L and δZ^R of the top quark wave function shown in Eqs.(2.13) and (2.14). The effect of the singularity makes the absolute value of the correction get a large increment near the singularity point. However at the gluino mass range which is far away from the singularity mass region, the correction approaches to a small value quickly. This implies that there exists decoupling with heavy gluino in the SUSY QCD corrections. The corresponding prediction for the CP-violation parameter ξ_{CP} as a function of $m_{\tilde{g}}$ is shown in Fig.4(b). There the singularity effect from the top quark wave function renormalization exists at the point $m_{\tilde{g}} = 75 \text{ GeV}$. The influence of the singularity also can be seen from the fact that in Fig.3(a)(b) the corrections are distinctly much smaller than those in Fig.2(a)(b). That is just because the parameters for Fig.3(a)(b) as shown in Eq.(3.3) are far away from the singularity point.

The relations between the corrections of the unpolarized cross section and the two stop quark masses $m_{\tilde{t}_1}$ and $m_{\tilde{t}_2}$ are depicted in Fig.5(a) and Fig.6(a) respectively. In Fig.5(a), the large corrections near the point $m_{\tilde{t}_1} = 75 \text{ GeV}$ are again due to the influence of the singularity. However, the corrections show the decoupling with the masses of stop quarks, when $m_{\tilde{t}_i}$ ($i = 1, 2$) are far away from the singularity points $m_{\tilde{t}_i} = m_t - m_{\tilde{g}}$. The decoupling effect can be seen more clearly in the heavy stop case. In Fig.6(a) the curves of corrections are rather flat in the heavy \tilde{t}_2 region,

and the small waves around $m_{\tilde{t}_2} = 250 \text{ GeV}$ are merely due to the resonance effect when $\sqrt{\hat{s}} = 2m_{\tilde{t}_2}$. The corresponding dependence of parameter ξ_{CP} on these two stop quark masses is given in Fig.5(b),6(b).

Fig.4(a), Fig.5(a) and Fig.6(a) also show clearly that the absolute corrections for $\phi = 45^\circ$ are apparently smaller than those for $\phi = 0^\circ$ in unpolarized photon fusion, except in the light gluino mass region in Fig.4(a) which is simply due to the singularity effect in top quark wave function renormalization. The fact that the corrections are always maximal for vanishing CP violation is simply due to the fact that with introducing a non-zero CP-violating phase angle in the gluino-stop-top coupling, the real part of this coupling strength will be reduced down quantitatively. Further analyses show that this reduction will lead a decrease in the absolute values of the real parts of form factors, whereas the imaginary parts of form factors do not contribute to the cross section. But around $m_{\tilde{t}_1} \sim \sqrt{\hat{s}}/2$ mass region shown in Fig.5(a), the situation is more complicated and this feature does not exist.

IV. Conclusion

In this work we have studied the one-loop supersymmetric QCD corrections of the process $\gamma(\lambda_2)\gamma(\lambda_1) \rightarrow t\bar{t}$.

From the results of numerical calculation, we can conclude that the singularity of the top quark wave function renormalization affects the corrections heavily. Large corrections can be expected near the singularity region which satisfies $m_t = m_{\tilde{g}} + m_{\tilde{t}_i}$ ($i = 1, 2$). This effect is shown in Fig.4(a), 5(a) and 6(a), where the large

corrections are all due to the singularity effect. This singularity effect can be also used to explain why the corrections are large in Fig.2(a), whereas the corrections in Fig.3(a) are small where the parameters are far away from all the singularity points. However the corrections are insensitive to the masses of supersymmetric particles \tilde{t}_i ($i = 1, 2$) and \tilde{g} when their masses are heavy and far away from singularity points. This feature is just the manifestation of the decoupling effects.

In any case, with the fusion of photons polarized with parallel spin directions, the corrections are always significant near the $t\bar{t}$ threshold. Furthermore, if the CP-violating phase really exists in the squark mixing matrix or in the Majorana mass term of the gluino predicted by the MSSM, the CP-violating parameter could be expected to be the order of $10^{-3} \sim 10^{-2}$. Therefore testing CP-violation in this process is one of the promising tasks for a future photon-photon collider.

This work was supported in part by the National Natural Science Foundation of China and the National Committee of Science and Technology of China. Part of this work was done when two of the authors, Ma Wen-Gan and Yu Zeng-Hui, visited the University Vienna under the exchange agreement (project number: IV.B.12).

Appendix

The form factors $f_{i,N}^{s(\hat{t})}$ can be expressed as

$$\begin{aligned}
 f_{1,R}^{s(\hat{t})} &= \frac{g_s^2 C_F}{4\pi^2} (p_2 \cdot p_4) \left\{ A_L B_R m_t B_1[-p_2 + p_4, m_{\tilde{g}}, m_{\tilde{t}_1}] + (L \leftrightarrow R, m_{\tilde{t}_1} \rightarrow m_{\tilde{t}_2}) \right\} \\
 &- \frac{g_s^2 C_F}{4\pi^2} (p_2 \cdot p_4) A_L B_L \left\{ m_{\tilde{g}} B_0[-p_2 + p_4, m_{\tilde{g}}, m_{\tilde{t}_1}] + (m_{\tilde{g}} \rightarrow -m_{\tilde{g}}, m_{\tilde{t}_1} \rightarrow m_{\tilde{t}_2}) \right\} \\
 &+ 2(p_2 \cdot p_4)(C_S^- - m_t C_R)
 \end{aligned} \tag{A1}$$

$$\begin{aligned}
 f_{2,R}^{s(\hat{t})} &= \frac{g_s^2 C_F}{4\pi^2} \left\{ (2A_L B_R p_2 \cdot p_4 - m_t^2) B_1[-p_2 + p_4, m_{\tilde{g}}, m_{\tilde{t}_1}] + (L \leftrightarrow R, m_{\tilde{t}_1} \rightarrow m_{\tilde{t}_2}) \right\} \\
 &+ \frac{g_s^2 C_F}{4\pi^2} (A_L B_L + A_R B_R) m_t \left\{ m_{\tilde{g}} B_0[-p_2 + p_4, m_{\tilde{g}}, m_{\tilde{t}_1}] + (m_{\tilde{g}} \rightarrow -m_{\tilde{g}}, m_{\tilde{t}_1} \rightarrow m_{\tilde{t}_2}) \right\} \\
 &- 2m_t (C_S^- + C_S^+) + 2m_t^2 (C_L + C_R) - 4(p_2 \cdot p_4) C_R
 \end{aligned} \tag{A2}$$

$$f_{3,R}^{s(\hat{t})} = \frac{1}{2} f_{2,R}^{s(\hat{t})} \tag{A3}$$

$$f_{i,L}^{s(\hat{t})} = f_{i,R}^{s(\hat{t})} (R \leftrightarrow L, C_S^+ \leftrightarrow C_S^-) \tag{A4}$$

where the definitions of the renormalization quantities C_S^\pm and $C_{R,L}$ can be found in Eq.(2.11), and those of $A_{R,L}$ and $B_{R,L}$ in Eq.(2.3). The replacement $m_{\tilde{g}} \rightarrow -m_{\tilde{g}}$ is not performed on the argument of loop integral functions B , C and D .

The form factors of triangle, vertex and box diagrams are given as follows

$$\begin{aligned}
 f_R^{tr} &= \frac{m_t C_F}{4} \left\{ (A_R B_L C_{11} - A_R B_L C_{12} + A_L B_R C_{12})[-p_2, p_1 + p_2, m_{\tilde{g}}, m_{\tilde{t}_1}, m_{\tilde{t}_1}] \right. \\
 &\quad \left. + (L \leftrightarrow R, m_{\tilde{t}_1} \rightarrow m_{\tilde{t}_2}) \right\} \\
 &- \frac{C_F}{4} A_L B_L \left\{ m_{\tilde{g}} C_0[-p_2, p_1 + p_2, m_{\tilde{g}}, m_{\tilde{t}_1}, m_{\tilde{t}_1}] \right. \\
 &\quad \left. + (m_{\tilde{g}} \rightarrow -m_{\tilde{g}}, m_{\tilde{t}_1} \rightarrow m_{\tilde{t}_2}) \right\}
 \end{aligned} \tag{A5}$$

$$f_L^{tr} = f_R^{tr}(R \leftrightarrow L) \quad (A6)$$

$$\begin{aligned} f_{1,R}^{v(\hat{t})} &= \frac{g_s^2 C_F}{4\pi^2} m_t \left\{ (A_L B_R - A_R B_L) C_{24} [-p_2, p_4, m_{\tilde{g}}, m_{\tilde{t}_1}, m_{\tilde{t}_1}] + (L \leftrightarrow R, m_{\tilde{t}_1} \rightarrow m_{\tilde{t}_2}) \right\} \\ &+ m_t (C_R - C_L) \end{aligned} \quad (A7)$$

$$f_{2,R}^{v(\hat{t})} = -\frac{g_s^2 C_F}{4\pi^2} 2(p_1 \cdot p_3) \left\{ A_L B_R (C_{12} + C_{23}) [p_1, -p_3, m_{\tilde{g}}, m_{\tilde{t}_1}, m_{\tilde{t}_1}] + (L \leftrightarrow R, m_{\tilde{t}_1} \rightarrow m_{\tilde{t}_2}) \right\} \quad (A8)$$

$$\begin{aligned} f_{3,R}^{v(\hat{t})} &= \frac{g_s^2 C_F}{4\pi^2} \left\{ (4A_L B_R C_{24} - m_t^2 (C_{11} + C_{21}) + 2 p_2 \cdot p_4 A_L B_R (C_{12} + C_{23})) [-p_2, p_4, m_{\tilde{g}}, m_{\tilde{t}_1}, m_{\tilde{t}_1}] + \right. \\ &\quad \left. (L \leftrightarrow R, m_{\tilde{t}_1} \rightarrow m_{\tilde{t}_2}) \right\} \\ &+ \frac{g_s^2 C_F}{4\pi^2} m_t (A_L B_L + A_R B_R) \left\{ m_{\tilde{g}} (C_0 + C_{11}) [-p_2, p_4, m_{\tilde{g}}, m_{\tilde{t}_1}, m_{\tilde{t}_1}] + (m_{\tilde{g}} \rightarrow -m_{\tilde{g}}, m_{\tilde{t}_1} \rightarrow m_{\tilde{t}_2}) \right\} \\ &+ 4C_R \end{aligned} \quad (A9)$$

$$\begin{aligned} f_{4,R}^{v(\hat{t})} &= \frac{g_s^2 C_F}{2\pi^2} m_t \left\{ (A_L B_R C_{11} + A_R B_L C_{12} - A_L B_R C_{12} + A_L B_R C_{21} + \right. \\ &\quad \left. A_R B_L C_{23} - A_L B_R C_{23}) [p_1, -p_3, m_{\tilde{g}}, m_{\tilde{t}_1}, m_{\tilde{t}_1}] + (L \leftrightarrow R, m_{\tilde{t}_1} \rightarrow m_{\tilde{t}_2}) \right\} \\ &- \frac{g_s^2 C_F}{2\pi^2} A_L B_L \left\{ m_{\tilde{g}} (C_0 + C_{11}) [p_1, -p_3, m_{\tilde{g}}, m_{\tilde{t}_1}, m_{\tilde{t}_1}] + (m_{\tilde{g}} \rightarrow -m_{\tilde{g}}, m_{\tilde{t}_1} \rightarrow m_{\tilde{t}_2}) \right\} \end{aligned} \quad (A10)$$

$$\begin{aligned} f_{5,R}^{v(\hat{t})} &= \frac{g_s^2 C_F}{2\pi^2} \left\{ A_L B_R C_{24} [-p_2, p_4, m_{\tilde{g}}, m_{\tilde{t}_1}, m_{\tilde{t}_1}] + (L \leftrightarrow R, m_{\tilde{t}_1} \rightarrow m_{\tilde{t}_2}) \right\} \\ &+ 2C_R \end{aligned} \quad (A11)$$

$$f_{6,R}^{v(\hat{t})} = \frac{1}{2} f_{4,R}^{v(\hat{t})} \quad (A12)$$

$$\begin{aligned}
f_{7,R}^{v(\hat{t})} &= \frac{g_s^2 C_F}{4\pi^2} m_t \{ (A_R B_L C_{11} - A_R B_L C_{12} + A_L B_R C_{12} + A_R B_L C_{21} - \\
&\quad A_R B_L C_{23} + A_L B_R C_{23}) [-p_2, p_4, m_{\bar{g}}, m_{\tilde{t}_1}, m_{\tilde{t}_1}] + (L \leftrightarrow R, m_{\tilde{t}_1} \rightarrow m_{\tilde{t}_2}) \} \\
&- \frac{g_s^2 C_F}{4\pi^2} A_L B_L \{ m_{\bar{g}} (C_0 + C_{11}) [-p_2, p_4, m_{\bar{g}}, m_{\tilde{t}_1}, m_{\tilde{t}_1}] + (m_{\bar{g}} \rightarrow -m_{\bar{g}}, m_{\tilde{t}_1} \rightarrow m_{\tilde{t}_2}) \}
\end{aligned} \tag{A13}$$

$$f_{i,L}^{v(\hat{t})} = f_{i,R}^{v(\hat{t})} (R \leftrightarrow L, C_S^+ \leftrightarrow C_S^-) \tag{A14}$$

$$\begin{aligned}
f_{7,R}^{b(\hat{t})} &= \frac{C_F}{8} m_t \{ (A_R B_L D_{311} - A_R B_L D_{313} + A_L B_R D_{313}) \\
&\quad [-p_2, p_4, p_3, m_{\bar{g}}, m_{\tilde{t}_1}, m_{\tilde{t}_1}, m_{\tilde{t}_1}] + (L \leftrightarrow R, m_{\tilde{t}_1} \rightarrow m_{\tilde{t}_2}) \} \\
&- \frac{C_F}{8} A_L B_L \{ m_{\bar{g}} D_{27} [-p_2, p_4, p_3, m_{\bar{g}}, m_{\tilde{t}_1}, m_{\tilde{t}_1}, m_{\tilde{t}_1}] + (m_{\bar{g}} \rightarrow -m_{\bar{g}}, m_{\tilde{t}_1} \rightarrow m_{\tilde{t}_2}) \}
\end{aligned} \tag{A15}$$

$$f_{2,R}^{b(\hat{t})} = f_{1,R}^{b(\hat{t})} \tag{A16}$$

$$\begin{aligned}
f_{3,R}^{b(\hat{t})} &= -\frac{C_F}{4} A_L B_R (D_{27} + D_{312}) [-p_2, p_4, p_3, m_{\bar{g}}, m_{\tilde{t}_1}, m_{\tilde{t}_1}, m_{\tilde{t}_1}] \\
&+ (L \leftrightarrow R, m_{\tilde{t}_1} \rightarrow m_{\tilde{t}_2})
\end{aligned} \tag{A17}$$

$$\begin{aligned}
f_{4,R}^{b(\hat{t})} &= -\frac{C_F}{4} A_L B_R D_{313} [-p_2, p_4, p_3, m_{\bar{g}}, m_{\tilde{t}_1}, m_{\tilde{t}_1}, m_{\tilde{t}_1}] \\
&+ (L \leftrightarrow R, m_{\tilde{t}_1} \rightarrow m_{\tilde{t}_2})
\end{aligned} \tag{A18}$$

$$\begin{aligned}
f_{5,R}^{b(\hat{t})} &= \frac{C_F}{4} A_L B_R (D_{311} - D_{312}) [-p_2, p_4, p_3, m_{\bar{g}}, m_{\tilde{t}_1}, m_{\tilde{t}_1}, m_{\tilde{t}_1}] \\
&+ (L \leftrightarrow R, m_{\tilde{t}_1} \rightarrow m_{\tilde{t}_2})
\end{aligned} \tag{A19}$$

$$\begin{aligned}
f_{6,R}^{b(\hat{t})} &= \frac{C_F}{4} A_L B_R (D_{27} + D_{311} - D_{313}) [-p_2, p_4, p_3, m_{\bar{g}}, m_{\tilde{t}_1}, m_{\tilde{t}_1}, m_{\tilde{t}_1}] \\
&+ (L \leftrightarrow R, m_{\tilde{t}_1} \rightarrow m_{\tilde{t}_2})
\end{aligned} \tag{A20}$$

$$\begin{aligned}
f_{7,R}^{b(\hat{t})} &= \frac{C_F}{4} m_t \{ (A_R B_L D_{23} - A_L B_R D_{23} - A_R B_L D_{25} - A_R B_L D_{310} + \\
&A_R B_L D_{39} - A_L B_R D_{39}) [-p_2, p_4, p_3, m_{\tilde{g}}, m_{\tilde{t}_1}, m_{\tilde{t}_1}, m_{\tilde{t}_1}] \\
&+ (L \leftrightarrow R, m_{\tilde{t}_1} \rightarrow m_{\tilde{t}_2}) \} \\
&+ \frac{C_F}{4} A_L B_L \{ m_{\tilde{g}} (D_{13} + D_{26}) [-p_2, p_4, p_3, m_{\tilde{g}}, m_{\tilde{t}_1}, m_{\tilde{t}_1}, m_{\tilde{t}_1}] \\
&+ (m_{\tilde{g}} \rightarrow -m_{\tilde{g}}, m_{\tilde{t}_1} \rightarrow m_{\tilde{t}_2}) \}
\end{aligned} \tag{A21}$$

$$\begin{aligned}
f_{8,R}^{b(\hat{t})} &= \frac{C_F}{4} m_t \{ (A_R B_L D_{35} - A_R B_L D_{310} - A_R B_L D_{37} + A_L B_R D_{37} + \\
&A_R B_L D_{39} - A_L B_R D_{39}) [-p_2, p_4, p_3, m_{\tilde{g}}, m_{\tilde{t}_1}, m_{\tilde{t}_1}, m_{\tilde{t}_1}] \\
&+ (L \leftrightarrow R, m_{\tilde{t}_1} \rightarrow m_{\tilde{t}_2}) \} \\
&- \frac{C_F}{4} A_L B_L \{ m_{\tilde{g}} (D_{25} - D_{26}) [-p_2, p_4, p_3, m_{\tilde{g}}, m_{\tilde{t}_1}, m_{\tilde{t}_1}, m_{\tilde{t}_1}] \\
&+ (m_{\tilde{g}} \rightarrow -m_{\tilde{g}}, m_{\tilde{t}_1} \rightarrow m_{\tilde{t}_2}) \}
\end{aligned} \tag{A22}$$

$$\begin{aligned}
f_{9,R}^{b(\hat{t})} &= \frac{C_F}{4} m_t \{ (A_R B_L D_{11} - A_R B_L D_{13} + A_L B_R D_{13} + A_R B_L D_{21} + \\
&A_R B_L D_{23} - A_L B_R D_{23} + A_R B_L D_{24} - 2A_R B_L D_{25} + \\
&A_L B_R D_{25} - A_R B_L D_{26} + A_L B_R D_{26} - 2A_R B_L D_{310} + \\
&A_L B_R D_{310} + A_R B_L D_{34} + A_R B_L D_{39} - A_L B_R D_{39}) \\
&[-p_2, p_4, p_3, m_{\tilde{g}}, m_{\tilde{t}_1}, m_{\tilde{t}_1}, m_{\tilde{t}_1}] \\
&+ (L \leftrightarrow R, m_{\tilde{t}_1} \rightarrow m_{\tilde{t}_2}) \} \\
&- \frac{C_F}{4} A_L B_L \{ m_{\tilde{g}} (D_0 + D_{11} + D_{12} - D_{13} + D_{24} - D_{26}) \\
&[-p_2, p_4, p_3, m_{\tilde{g}}, m_{\tilde{t}_1}, m_{\tilde{t}_1}, m_{\tilde{t}_1}] \\
&+ (m_{\tilde{g}} \rightarrow -m_{\tilde{g}}, m_{\tilde{t}_1} \rightarrow m_{\tilde{t}_2}) \}
\end{aligned} \tag{A23}$$

$$\begin{aligned}
f_{10,R}^{b(\hat{t})} &= \frac{C_F}{4} m_t \{ (A_R B_L D_{24} - A_R B_L D_{21} + A_R B_L D_{25} - A_L B_R D_{25} - \\
&A_R B_L D_{26} + A_L B_R D_{26} - A_R B_L D_{31} - 2A_R B_L D_{310} + \\
&A_L B_R D_{310} + A_R B_L D_{34} + 2A_R B_L D_{35} - A_L B_R D_{35} - \\
&A_R B_L D_{37} + A_L B_R D_{37} + A_R B_L D_{39} - A_L B_R D_{39}) \\
&[-p_2, p_4, p_3, m_{\tilde{g}}, m_{\tilde{t}_1}, m_{\tilde{t}_1}, m_{\tilde{t}_1}] \\
&+ (L \leftrightarrow R, m_{\tilde{t}_1} \rightarrow m_{\tilde{t}_2}) \} \\
&+ \frac{C_F}{4} A_L B_L \{ m_{\tilde{g}} (D_{11} - D_{12} + D_{21} - D_{24} - D_{25} + D_{26}) \\
&[-p_2, p_4, p_3, m_{\tilde{g}}, m_{\tilde{t}_1}, m_{\tilde{t}_1}, m_{\tilde{t}_1}] \\
&+ (m_{\tilde{g}} \rightarrow -m_{\tilde{g}}, m_{\tilde{t}_1} \rightarrow m_{\tilde{t}_2}) \}
\end{aligned} \tag{A24}$$

$$\begin{aligned}
f_{11,R}^{b(\hat{t})} &= -\frac{C_F}{8} A_L B_R (D_{312} - D_{313}) \\
&\quad [-p_2, p_4, p_3, m_{\bar{g}}, m_{\bar{t}_1}, m_{\bar{t}_1}, m_{\bar{t}_1}] \\
&+ (L \leftrightarrow R, m_{\bar{t}_1} \rightarrow m_{\bar{t}_2})
\end{aligned} \tag{A25}$$

$$f_{12,R}^{b(\hat{t})} = f_{11,R}^{b(\hat{t})} \tag{A26}$$

$$\begin{aligned}
f_{13,R}^{b(\hat{t})} &= \frac{C_F}{4} A_L B_R (D_{26} + D_{38} - D_{39} - D_{23}) \\
&\quad [-p_2, p_4, p_3, m_{\bar{g}}, m_{\bar{t}_1}, m_{\bar{t}_1}, m_{\bar{t}_1}] \\
&+ (L \leftrightarrow R, m_{\bar{t}_1} \rightarrow m_{\bar{t}_2})
\end{aligned} \tag{A27}$$

$$\begin{aligned}
f_{14,R}^{b(\hat{t})} &= \frac{C_F}{4} A_L B_R (D_{37} + D_{38} - D_{39} - D_{310}) \\
&\quad [-p_2, p_4, p_3, m_{\bar{g}}, m_{\bar{t}_1}, m_{\bar{t}_1}, m_{\bar{t}_1}] \\
&+ (L \leftrightarrow R, m_{\bar{t}_1} \rightarrow m_{\bar{t}_2})
\end{aligned} \tag{A28}$$

$$\begin{aligned}
f_{15,R}^{b(\hat{t})} &= \frac{C_F}{4} A_L B_R (D_{13} - D_{12} - D_{22} - D_{23} - D_{24} + D_{25} + \\
&\quad 2D_{26} + D_{310} - D_{36} + D_{38} - D_{39}) \\
&\quad [-p_2, p_4, p_3, m_{\bar{g}}, m_{\bar{t}_1}, m_{\bar{t}_1}, m_{\bar{t}_1}] \\
&+ (L \leftrightarrow R, m_{\bar{t}_1} \rightarrow m_{\bar{t}_2})
\end{aligned} \tag{A29}$$

$$\begin{aligned}
f_{16,R}^{b(\hat{t})} &= \frac{C_F}{4} A_L B_R (D_{24} - D_{22} - D_{25} + D_{26} + D_{34} - D_{35} - \\
&\quad D_{36} + D_{37} + D_{38} - D_{39}) \\
&\quad [-p_2, p_4, p_3, m_{\bar{g}}, m_{\bar{t}_1}, m_{\bar{t}_1}, m_{\bar{t}_1}] \\
&+ (L \leftrightarrow R, m_{\bar{t}_1} \rightarrow m_{\bar{t}_2})
\end{aligned} \tag{A30}$$

$$f_{i,L}^{b(\hat{t})} = f_{i,R}^{b(\hat{t})} (R \leftrightarrow L) \tag{A31}$$

where

$$(p_3 - p_1)^2 = \hat{t}, \quad \hat{s} = (p_1 + p_2)^2,$$

$$2p_1 \cdot p_3 = 2p_2 \cdot p_4 = m_t^2 - \hat{t},$$

$$2p_3 \cdot p_4 = \hat{s}, \quad 2p_1 \cdot p_4 = 2p_2 \cdot p_3 = m_t^2 - \hat{u}$$

$$2p_1 \cdot p_2 = \hat{s} - 2m_t^2, \quad \hat{s} + \hat{t} + \hat{u} = 2m_t^2.$$

All the definitions of loop integral functions A , B , C and D used in our paper can be found in Ref.[14]. The numerical calculation of the vector and tensor loop integral functions can be traced back to the four scalar loop integrals A_0 , B_0 , C_0 and D_0 in Ref.[15].

References

- [1] CDF Collaboration, F. Abe et al., Phys. Rev. Lett. 74,2626(1995); D0 Collaboration, S. Abachi et al., Phys. Rev. Lett. 74,2632(1995).
- [2] I.F. Ginzbyrg, G.L. Kotkin, V.G. Serbo and V.I. Telnov, Pis'ma ZHETF 34(1981)514; Nucl. Instr. Methods 205(1983)47.
- [3] Ma Wen-Gan, Li Chong-Sheng and Han Liang, Phys. Rev. D Vol.53, No.3; V. Barger and R.J.N. Phillips, Phys. Rev. D 39, 3310(1989); A.C. Bawa et al, Z. Phys. C 47, 75(1990); Han Liang, Cheng-Guo Hu, Chong-Sheng Li and Ma Wen-Gan, Phys. Rev. D54(1996)2363.
- [4] O.J.P. Eboli et al.,Phys.Rev.**D47**,(1993)1889.
- [5] B. Kamal, Z. Merebashvili and A.P. Contogouris, Phy. Rev. D Vol.51, No.9(1995)4808
- [6] H.E. Haber and G. Kane, Phys. Rep. 117(1985)75; J.Gunion and H.E. Haber, Nucl. Phys. B272(1986)1.
- [7] H. Wang, C.S. Li et al, TUIMP-TH-95/76
- [8] S.J. Brodsky, P.M. Zerwas, Nucl. Instr. and Meth. A355(1995).
- [9] Ma Wen-Gan, Chang Chao-Hsi, Li Xue-Qian, Han Liang and Yu Zeng-Hui, AS-ITP-96-05, March, 1996; AS-ITP-96-06, March, 1996 (to be appeared on Commun. of Theor. Phys.).

- [10] M. Dugan, B. Grinshtein and L. Hall, Nucl. Phys. B255(1985)413; W. Bernreuther and M. Suzuki, Rev. Mod. Phys. 63(1991)313.
- [11] A. Denner, Fortsch. Phys. Vol.41, No.4 (1993)
- [12] Bernd A. Kniehl and A. Pilaftsis, Nucl. Phys. B474(1996)286.
- [13] the L3 Collaboration, CERN-PPE/96-29(Submitted to Phys. Lett.B)
- [14] Bernd A. Kniehl, Phys. Rep. 240(1994)211.
- [15] G. Passarino and M. Veltman, Nucl. Phys. B160(1979)151.

Figure Captions

Fig.1 Feynman diagrams for contributions from the tree-level and next-to-leading order in Supersymmetric QCD for the $\gamma\gamma \rightarrow t\bar{t}$ process: (a-b) tree level diagrams; (c-e) self-energy diagrams; (f-g) vertex diagrams; (h) box diagrams; (i) triangle diagrams. The dashed lines represent \tilde{t}_1, \tilde{t}_2 for (c-i).

Fig.2 With $m_{\tilde{g}} = m_{\tilde{t}_1} = 100 \text{ GeV}$ and $m_{\tilde{t}_2} = 450 \text{ GeV}$: (a) the cross section of the $t\bar{t}$ production process $\sigma(\pm\pm)$ as a function of $\sqrt{\hat{s}}$, solid line for tree-level contribution, dotted line for the MSSM correction with $\phi = 0^\circ$, dashed line for the MSSM correction with $\gamma(+)\gamma(+)$ polarization and $\phi = 45^\circ$, dash-dotted line for the MSSM correction with $\gamma(-)\gamma(-)$ polarization and $\phi = 45^\circ$; (b) the cross section $\sigma(\pm\mp)$ as a function of $\sqrt{\hat{s}}$, solid line for tree level contribution, dotted line for the MSSM correction with $\phi = 0^\circ$, dashed line for the MSSM correction with $\phi = 45^\circ$; (c) the CP-violating parameter ξ_{CP} as a function of $\sqrt{\hat{s}}$.

Fig.3 With $m_{\tilde{g}} = 5 \text{ GeV}$, $m_{\tilde{t}_1} = 50 \text{ GeV}$ and $m_{\tilde{t}_2} = 250 \text{ GeV}$: (a) the relative corrections to the cross section of the $t\bar{t}$ production process $\sigma(\pm\pm)$ as a function of $\sqrt{\hat{s}}$, dotted line for the MSSM correction with $\phi = 0^\circ$, dashed line for the MSSM correction with $\gamma(+)\gamma(+)$ polarization and $\phi = 45^\circ$, dash-dotted line for the MSSM correction with $\gamma(-)\gamma(-)$ polarization and $\phi = 45^\circ$. (b) the relative corrections to the cross section $\sigma(\pm\mp)$ as a function of $\sqrt{\hat{s}}$, dotted line for the MSSM correction with $\phi = 0^\circ$, dashed line for the MSSM correction with $\phi = 45^\circ$; (c) the CP-violating parameter ξ_{CP} as a function of $\sqrt{\hat{s}}$.

Fig.4 With $m_{\tilde{t}_1} = 100 \text{ GeV}$, $m_{\tilde{t}_2} = 450 \text{ GeV}$ and $\sqrt{\hat{s}} = 500 \text{ GeV}$: (a) the cross section σ of the $t\bar{t}$ production process from unpolarized photon collision as a function of $m_{\tilde{g}}$, solid line for tree level contribution, dotted line for the MSSM correction with $\phi = 0^\circ$, dashed line for the MSSM correction with $\phi = 45^\circ$; (b) the CP-violating parameter ξ_{CP} as a function of $m_{\tilde{g}}$.

Fig.5 With $m_{\tilde{g}} = 100 \text{ GeV}$, $m_{\tilde{t}_2} = 450 \text{ GeV}$ and $\sqrt{\hat{s}} = 500 \text{ GeV}$: (a) the cross section σ of the $t\bar{t}$ production process for unpolarized photon collision as a function of $m_{\tilde{t}_1}$, solid line for tree level contribution, dotted line for the MSSM correction with $\phi = 0^\circ$, dashed line for the MSSM correction with $\phi = 45^\circ$; (b) the CP-violating parameter ξ_{CP} as a function of $m_{\tilde{t}_1}$.

Fig.6 With $m_{\tilde{g}} = m_{\tilde{t}_1} = 100 \text{ GeV}$ and $\sqrt{\hat{s}} = 500 \text{ GeV}$: (a) the cross section σ of the $t\bar{t}$ production process from unpolarized photon collision as a function of $m_{\tilde{t}_2}$, solid line for tree level contribution, dotted line for the MSSM correction with $\phi = 0^\circ$, dashed line for the MSSM correction with $\phi = 45^\circ$; (b) the CP-violating parameter ξ_{CP} as a function of $m_{\tilde{t}_2}$.

Fig.2(a)

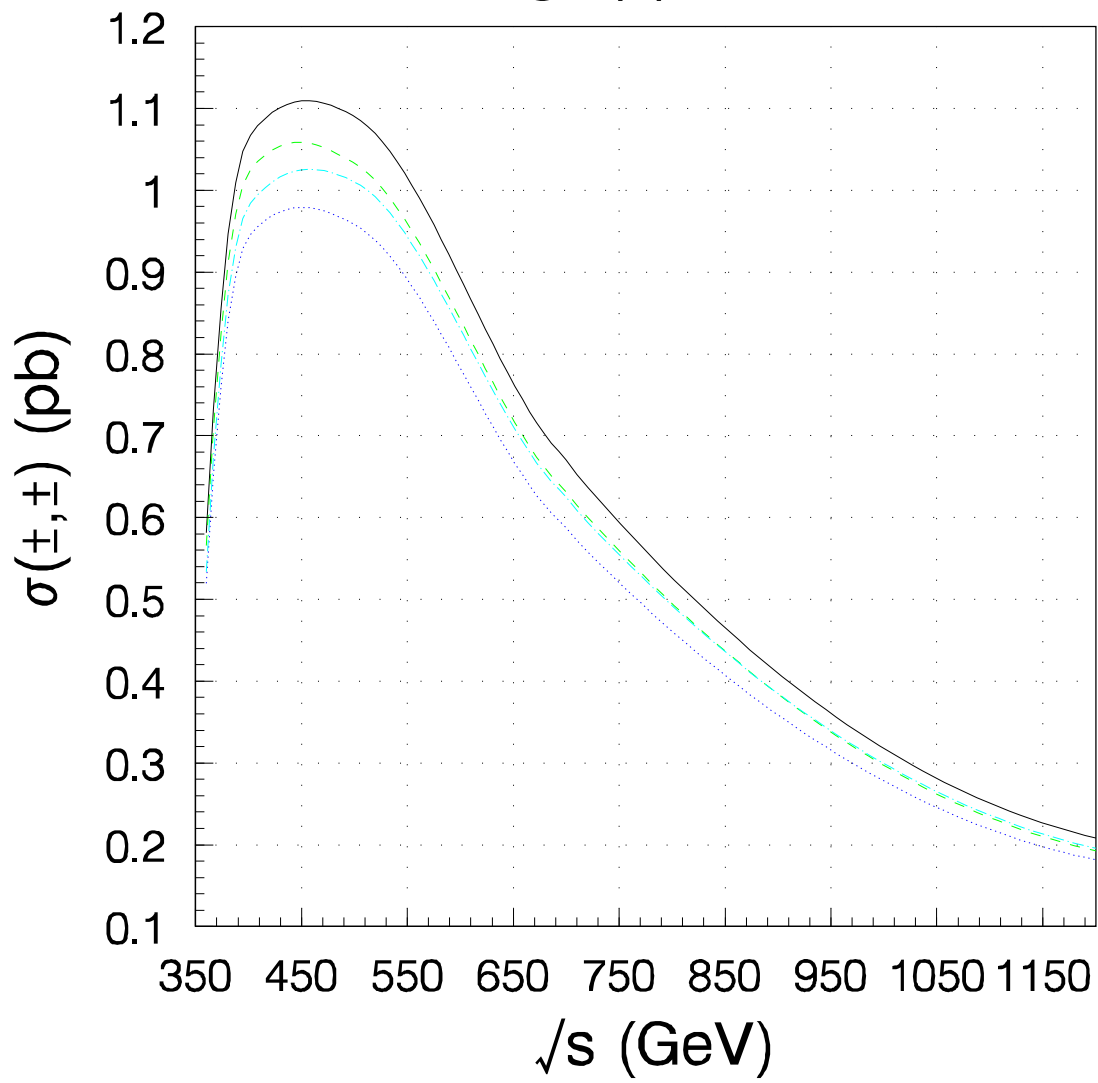


Fig.2(b)

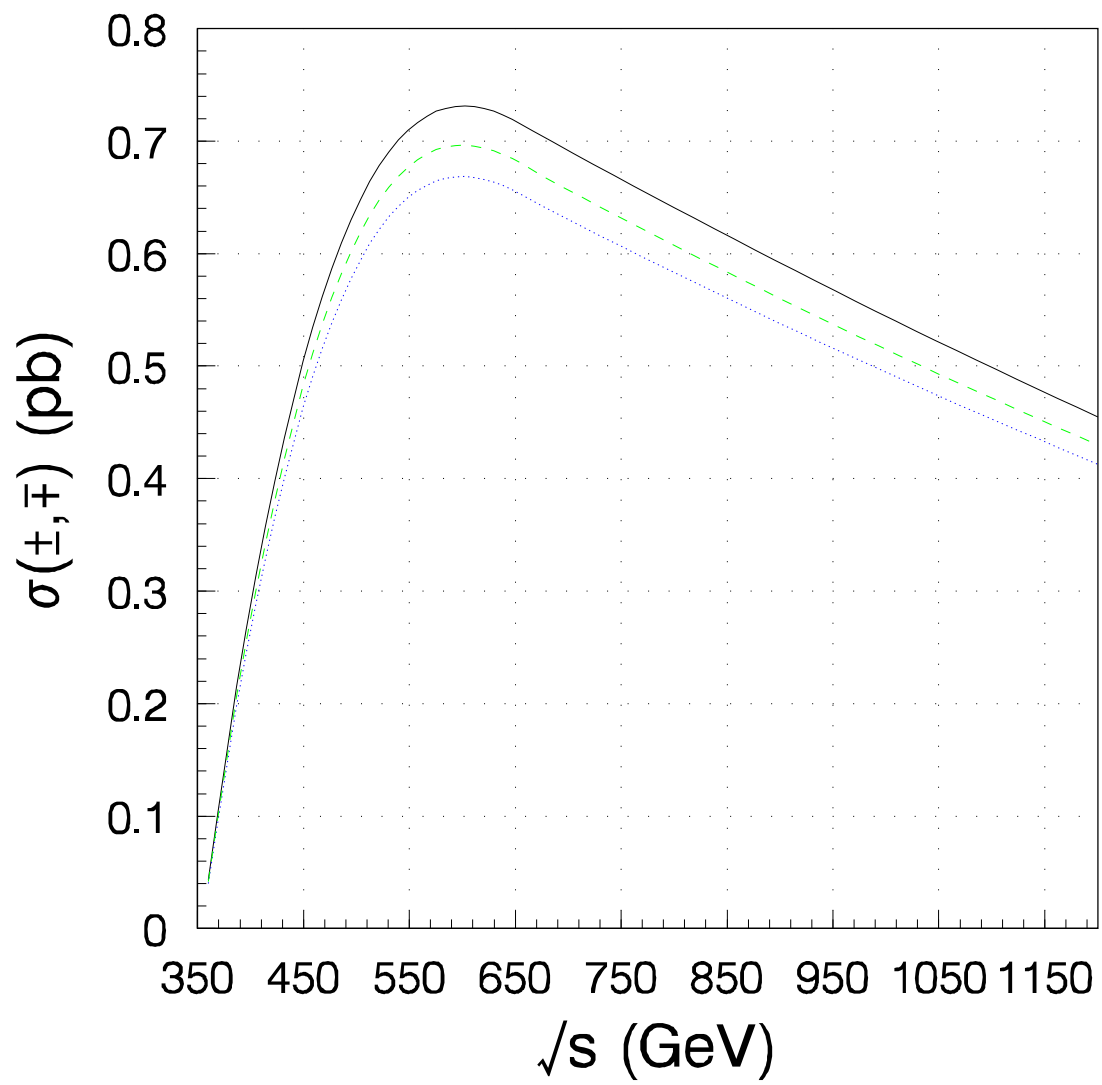


Fig.2(c)

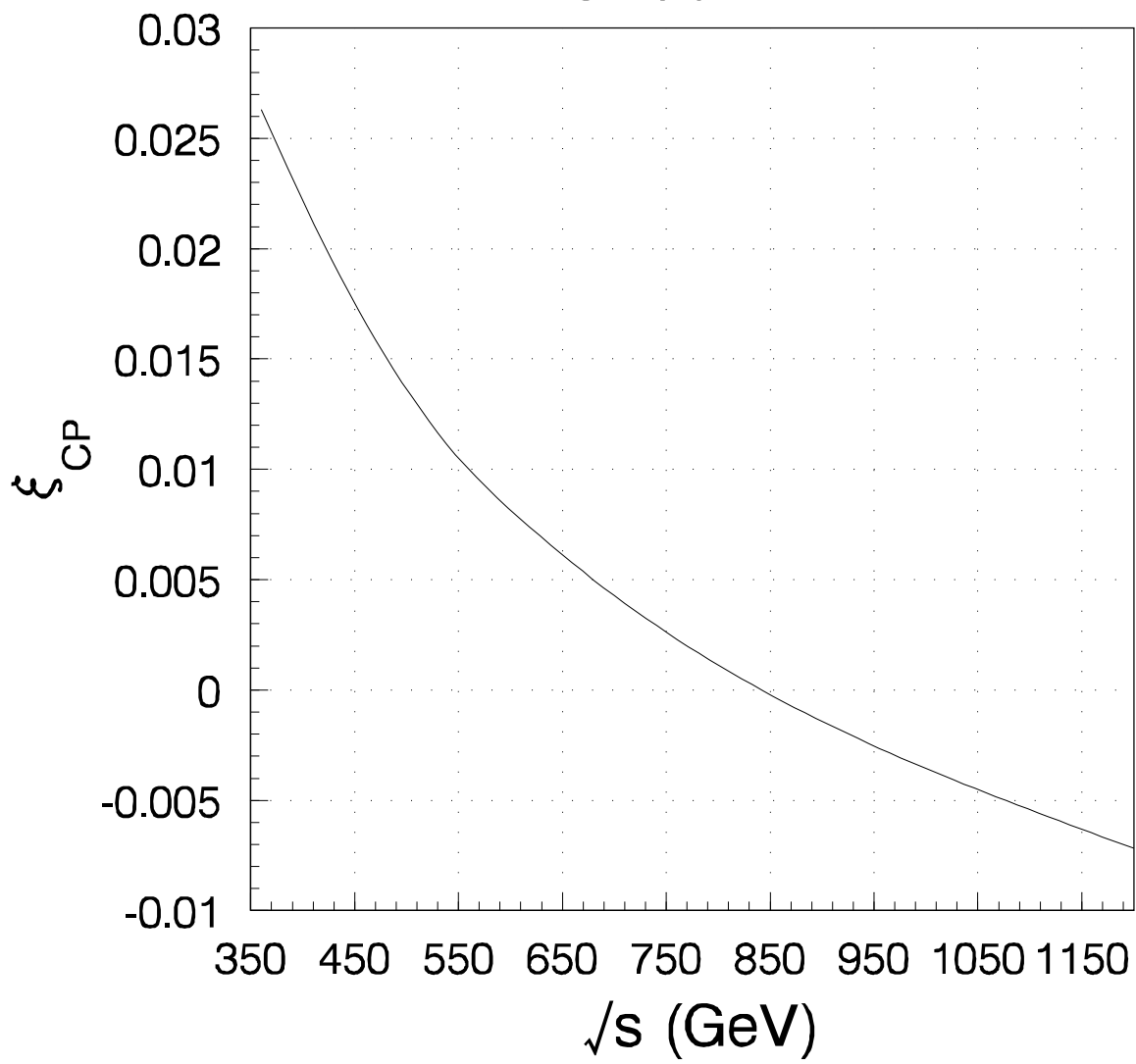


Fig.3(a)

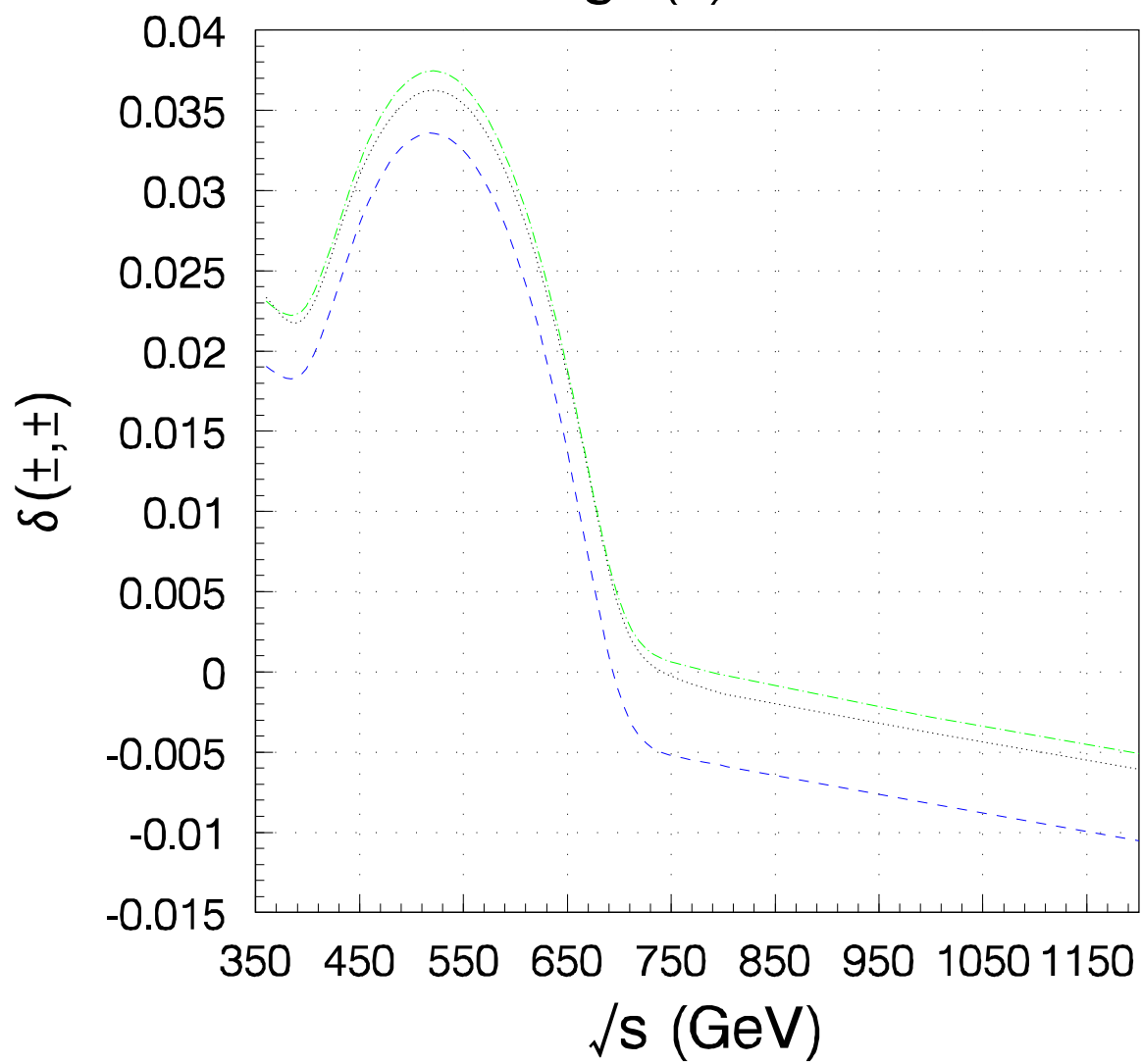


Fig.3(b)

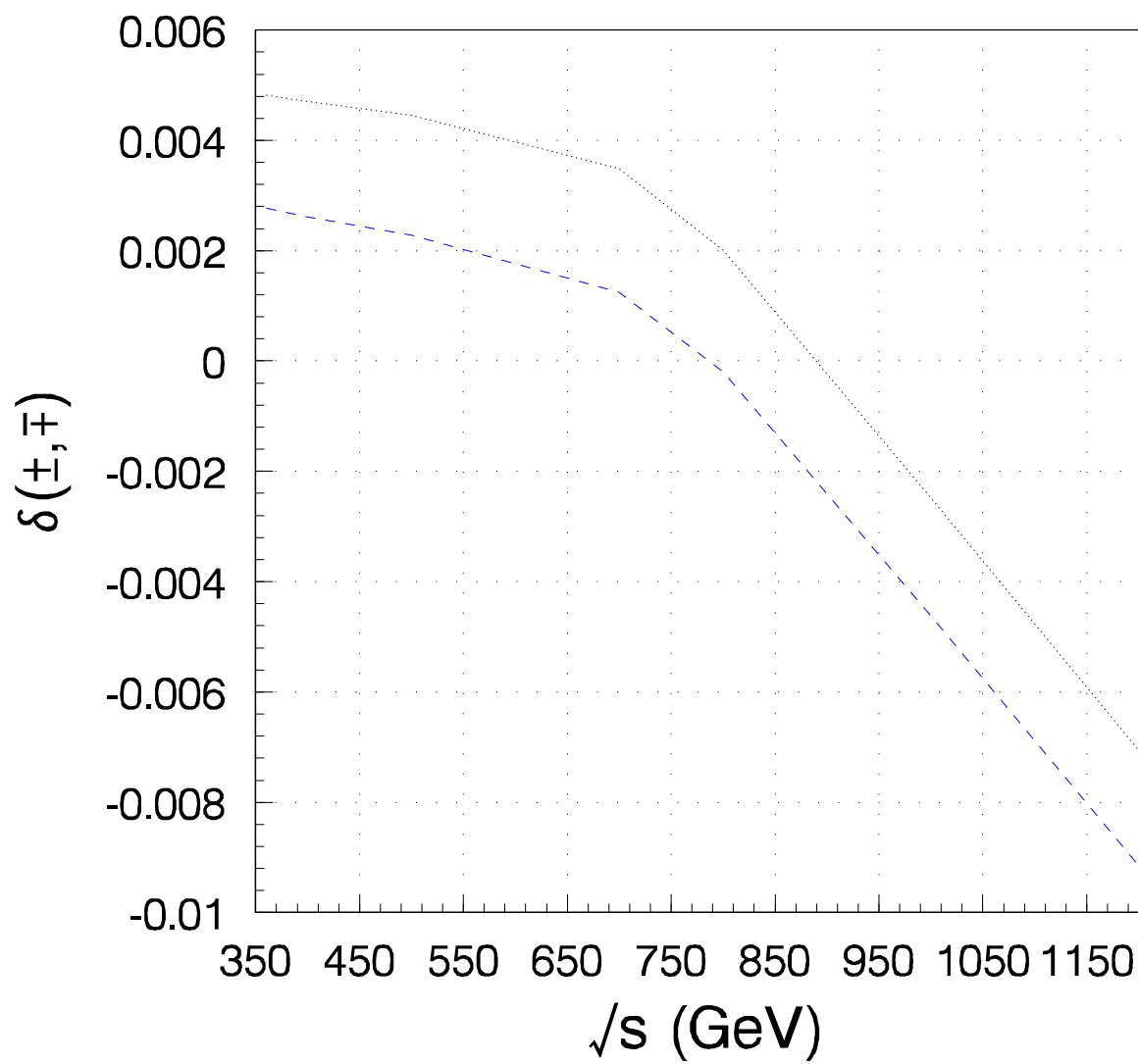


Fig.3(c)

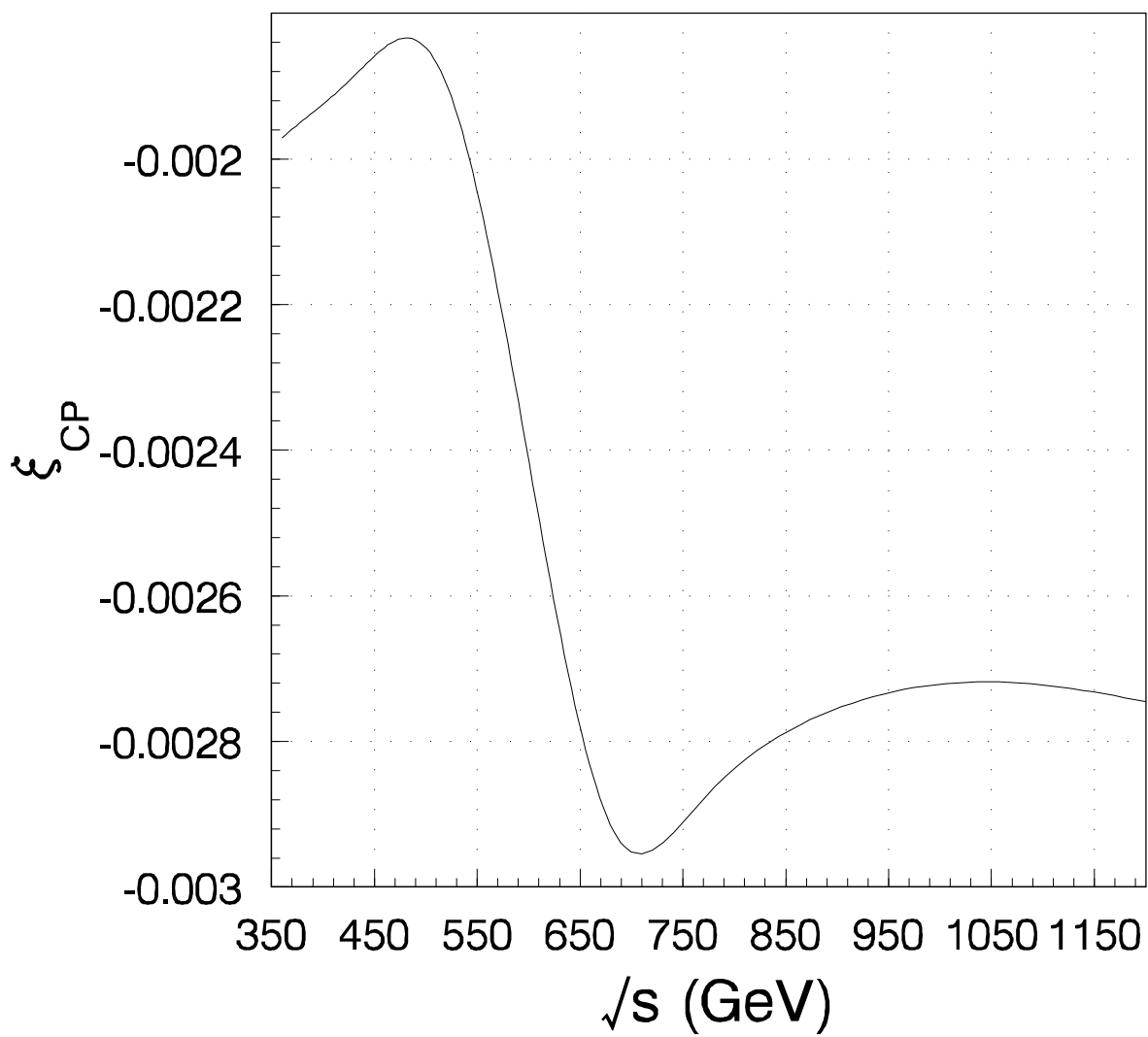


Fig.4(a)

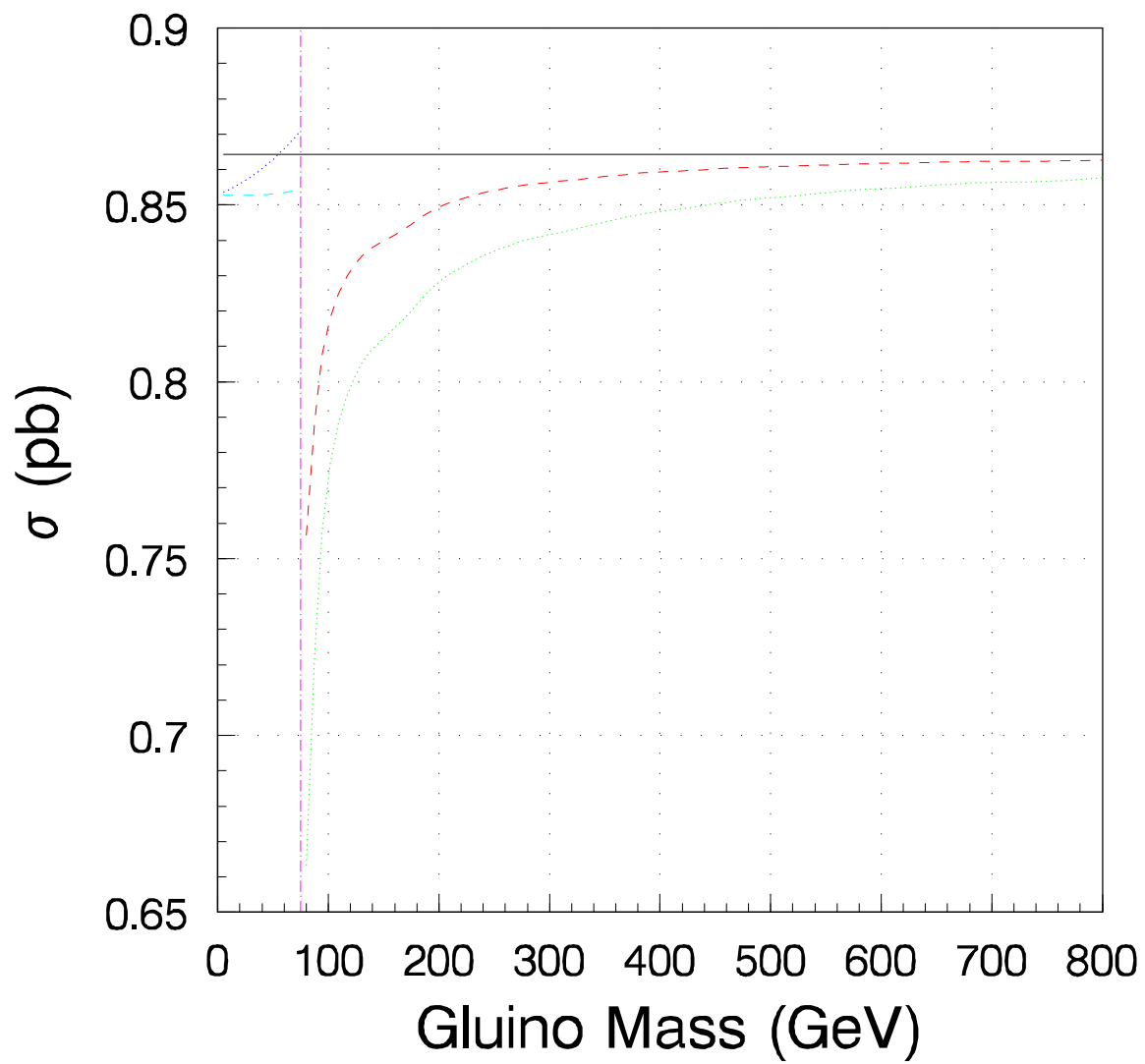


Fig.4(b)

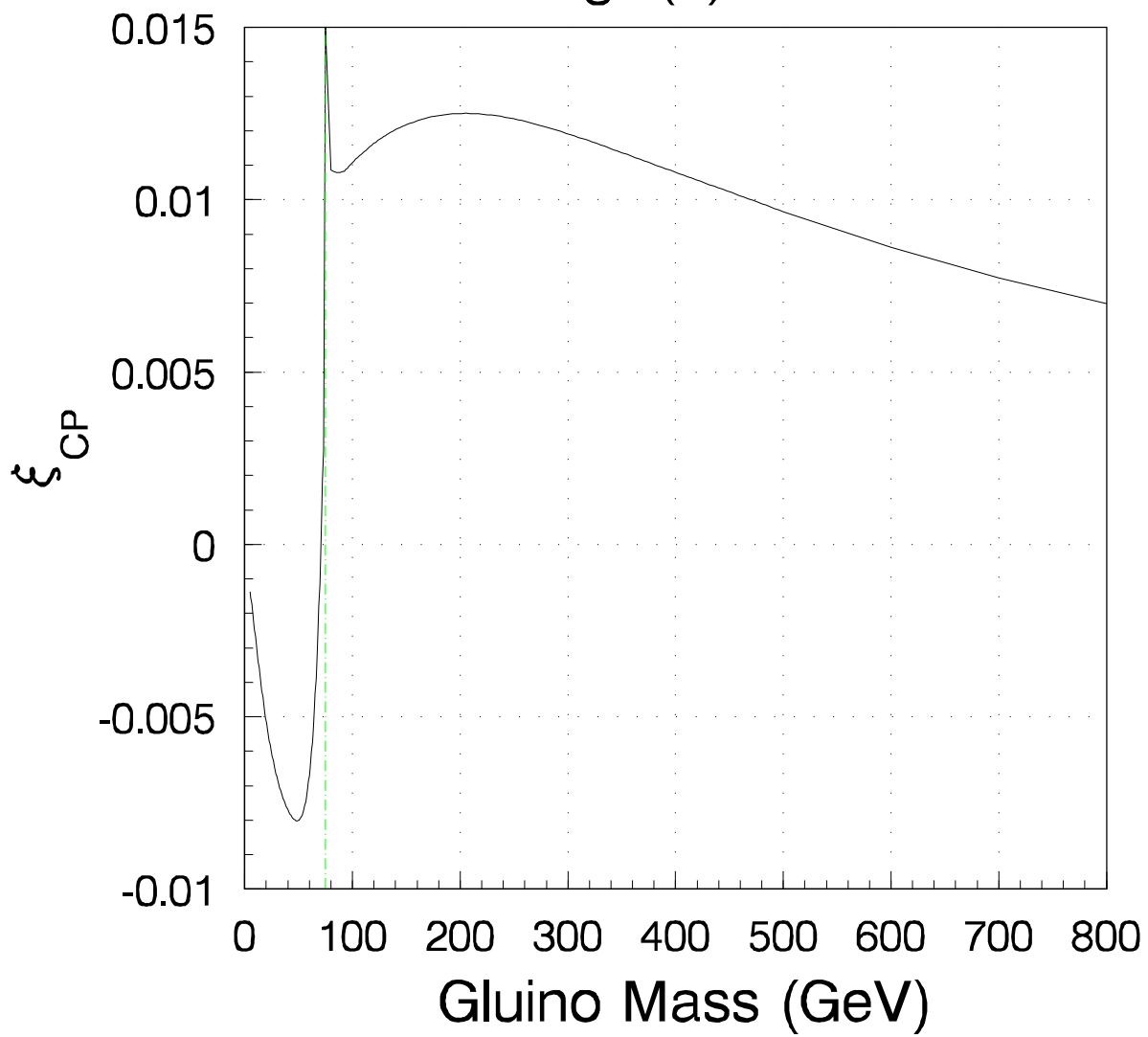


Fig.5(a)

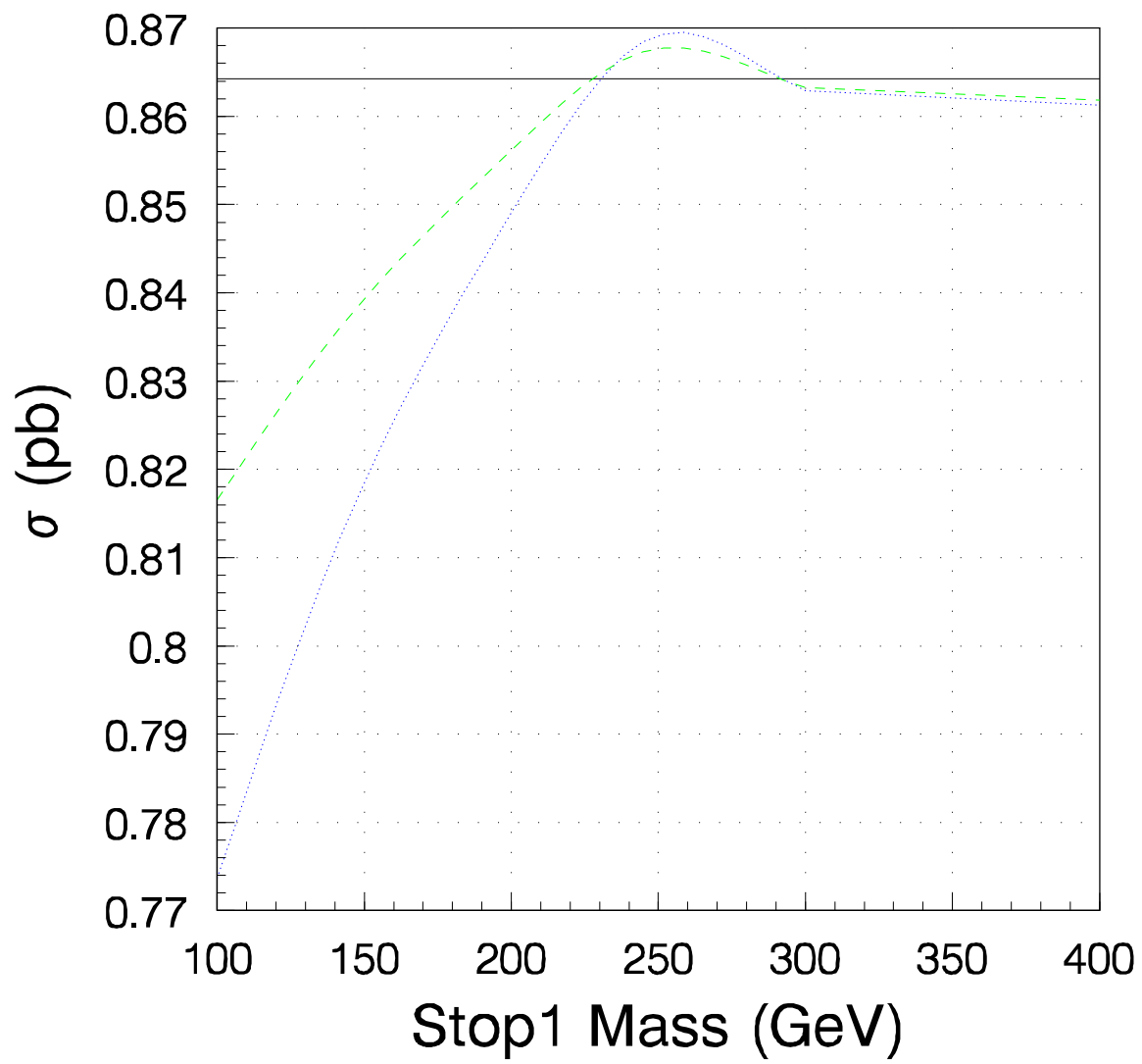


Fig.5(b)

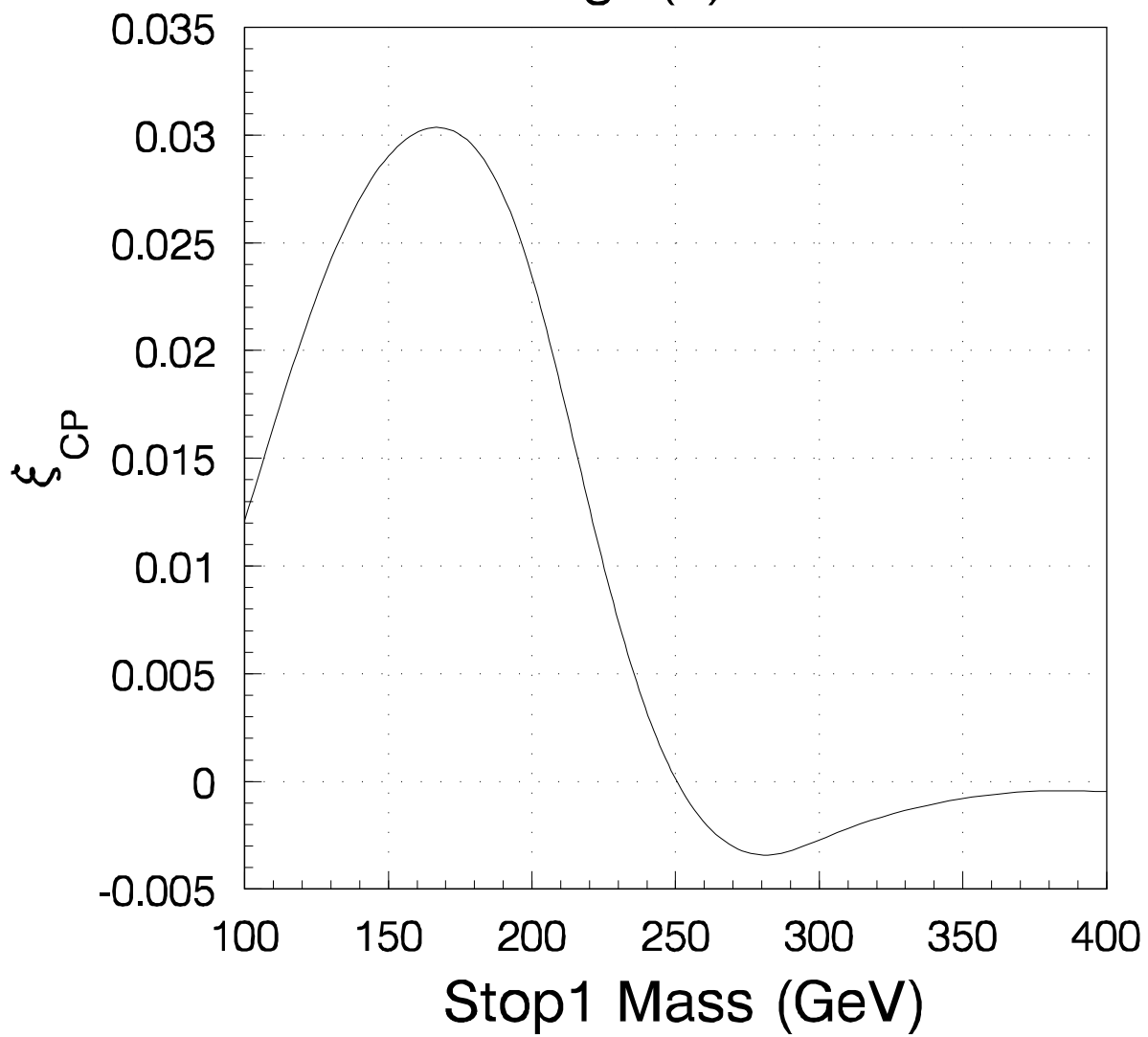


Fig.6(a)

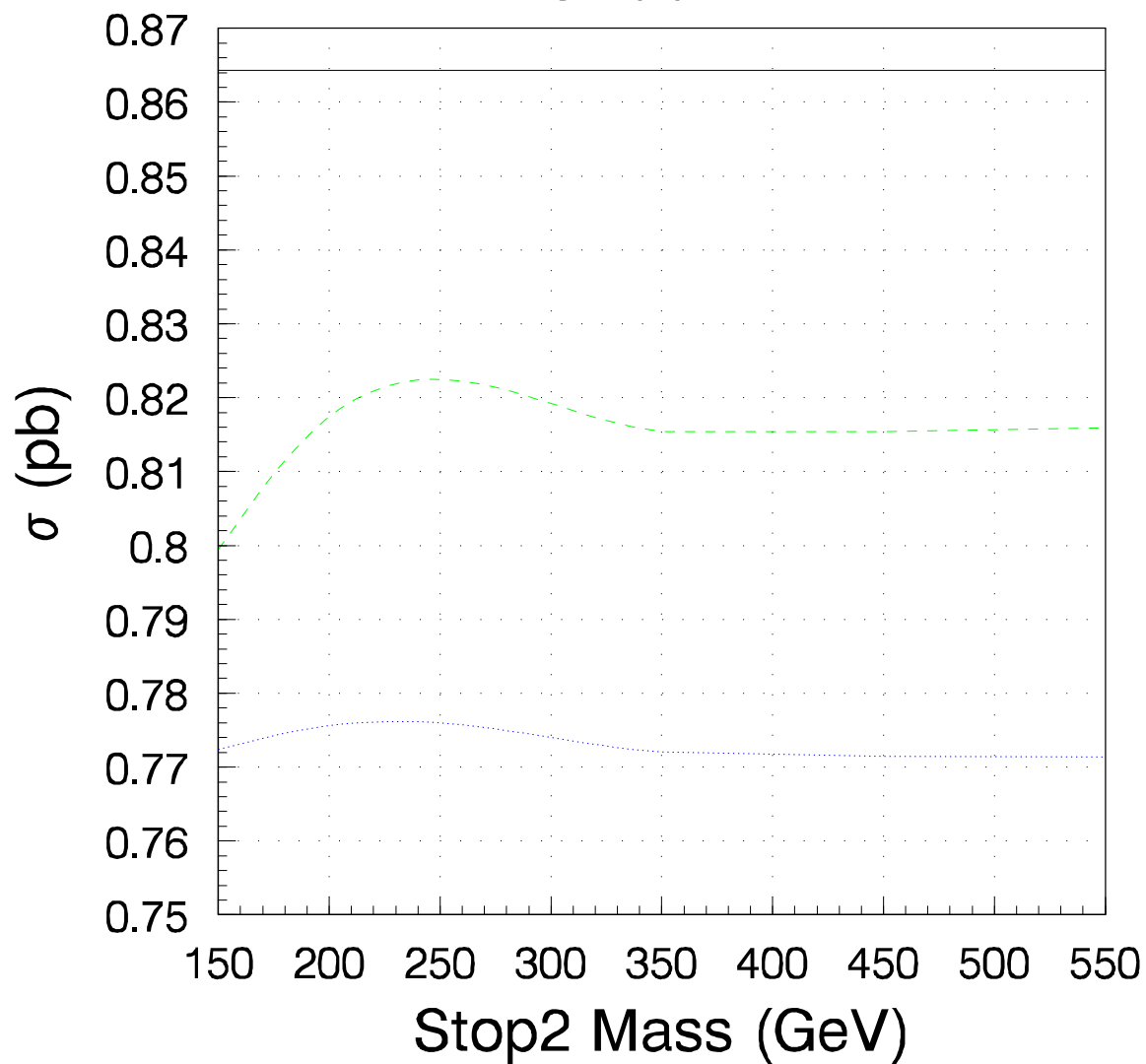


Fig.6(b)

